Progress In Electromagnetics Research, PIER 17, 1–24, 1997

AN R.F. SENSOR FOR LOGGING-WHILE-DRILLING GEOPHYSICAL MEASUREMENTS

T. M. de Swiet

Schlumberger-Doll Research
Old Quarry Road, Ridgefield
CT 06877-4108, USA

1. INTRODUCTION

Electrical measurements have been instrumental in geophysical exploration since the 1930's. Historically these measurements would be made by an apparatus or sonde lowered into a borehole after drilling had taken place. More recently, however, it has been increasingly common to make petrophysical measurements during the drilling process. One obvious advantage of such activity is that the data can be used to influence the direction in which the borehole is drilled.

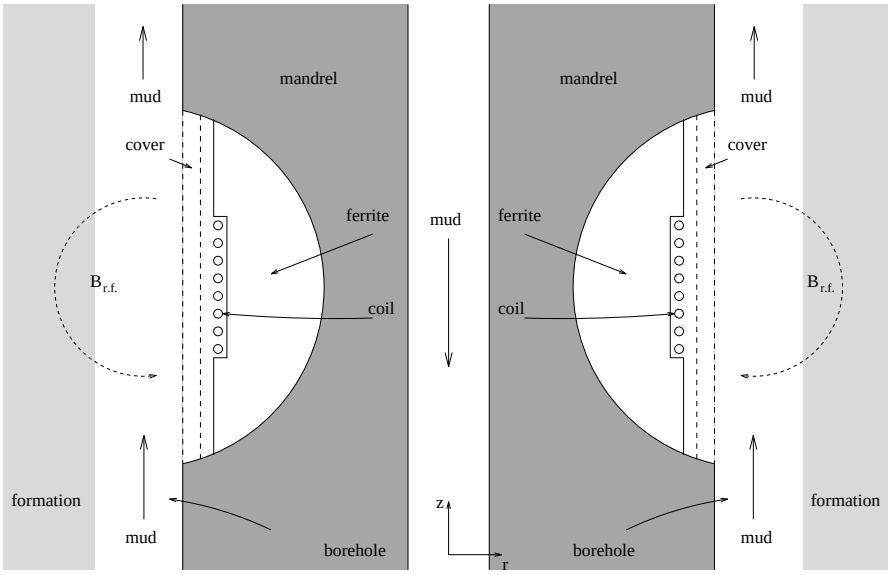

Figure 1. Schematic of R.F. Antenna.

This paper discusses the physics and aspects of the optimization of a type of near field radio frequency antenna which has been proposed for use in logging-while-drilling measurements. A numerical boundary element method is developed to provide accurate quantitative results.

A schematic of the kind of application that is being considered is shown in Fig. 1. Mounted on the rotating drill string, the antenna is approximately cylindrically symmetric. Thus Fig. 1 shows a cut through the antenna at a fixed azimuth. Drilling mud is circulated down the center of the drill string mandrel and up the outside. The antenna must be mounted on the metal cylindrical shell of the mandrel. The r.f. magnetic field that is necessary for the measurement must be created by an azimuthal current sheet of some kind. It is natural to use a coil wrapped around the mandrel for this purpose. Radio frequency magnetic flux cannot penetrate into the metal mandrel and so a recess must be cut into the mandrel, behind the antenna coil, through which the flux can pass. This recess is filled with ferrite ($\mu_r \sim 100$) in order to decrease its magnetic reluctance. There are tight restrictions on the allowed depth of the recess in order that the structural integrity

of the mandrel not be compromised. In addition it is essential that the antenna is protected by a strong cover from the hostile drilling environment. Within these constraints there remain many free design parameters. Examples include the dimensions and position of the coil, the axial extent of the recess, the option of copper plating certain parts of the mandrel and so on.

In the next section the theory of the numerical boundary element method is presented. This is followed by a discussion of the design optimization of the kind of device just mentioned. It is argued that the most important unconstrained degree of freedom is the axial extent of the antenna. Once this is set, there are several fine scale features that can be adjusted. The most interesting of these is the coil design, where the optimal number of coil turns is strongly influenced by 'proximity' effects. Such effects have been previously described by Smith [1] and others in relation to the problem of minimizing the a.c. resistance of a long multiwire transmission line.

2. THEORY

In this section, the numerical technique used to model the antenna performance, and the theory behind it are discussed. The goal of the numerical model is to be able to compute the magnetic field at any position, and, in addition, to compute circuit parameters such as the coil inductance, and dissipated power.

2.1 Simplifying Assumptions

1. The antenna is cylindrically symmetric. Azimuthal symmetry is in fact weakly broken by the pitch of the antenna coil, and the coupling of the r.f. power supply into the coil. In the cylindrical approximation the coil of the antenna must be approximated by a series of hoops of metal, with the current constrained to be equal in each hoop. The combination of cylindrical symmetry, and a purely azimuthal driving electric field, substituted into Maxwell's equations yield

$$\mathbf{E} = E_\phi(r,z)\hat{\phi} \ , \text{ and} \tag{1}$$

$$\mathbf{B} = \frac{-i}{\omega}\nabla \times \mathbf{E} = B_r(r,z)\hat{\mathbf{r}} + B_z(r,z)\hat{\mathbf{z}} \ . \tag{2}$$

2. The external wavelength is long. Displacement currents are utterly negligible at the expected operating frequencies. However the

conductivity of borehole fluid is typically in the 1 Sm^{-1} range. At 1MHz, the frequency considered in this paper, this leads to a wavevector of $\sim 2\,\mathrm{m}^{-1}$. Since typical antenna dimensions are expected to be of the order 10 cm, the long wavelength approximation will be inadequate in such cases. The effect of borehole conductivity will be discussed later. The long wavelength approximation implies that outside of metal parts the electric field satisfies

$$\nabla^2(E_\phi\hat{\phi}) = (\nabla^2 E_\phi - \frac{E_\phi}{r^2})\hat{\phi} = 0\ . \tag{3}$$

3. The skin depth is small in metallic elements. The skin depth in copper at 1 MHz is $\sim 0.06\,\mathrm{mm}$. This is small compared to almost all other length scales in the problem. Thus it is reasonable to compute the fields under the assumption that metal parts are perfect conductors and calculate the Ohmic dissipation afterwards as a perturbation [2]. A drawback of this method is that Ohmic losses are overestimated at sharp corners, where the surface current density diverges for perfect conductors. The magnetic field must be tangential to perfect metal conductors, thus at the surface of one of the metal parts of the antenna, where the local surface normal is $\hat{\mathbf{n}}$, $\mathbf{B}.\hat{\mathbf{n}} = 0$, which implies that

$$(\frac{E_\phi}{r} + \frac{\partial E_\phi}{\partial r})\hat{n}_z - \frac{\partial E_\phi}{\partial z}\hat{n}_r = 0\ , \tag{4}$$

which in turn implies that

$$E_\phi = \frac{C_i}{r}\ , \tag{5}$$

on all metal surfaces, where C_i is some constant. The significance of this constant is made clear by considering $\oint \mathbf{E}.d\mathbf{l} = 2\pi C_i$, where the contour of integration is a ring of fixed r and z on the metal surface. From Stoke's theorem, this integral is proportional to the magnetic flux through the ring. For a simply connected metal surface, such as the central mandrel in the antenna, there can be no flux through the ring, and so the constant C_i is zero. For a hoop of metal, such as a turn of the coil, the contour just mentioned can enclose flux and so C_i is in general non-zero. However, since the electric field is zero inside a perfect conductor, a non-zero C_i implies that there must be an e.m.f. of $2\pi C_i$ inside the hoop. Thus C_i is fixed by the source

electromotance, which in this cylindrically symmetric model, must be evenly distributed around any metal hoops. An interesting point is that one can expect this model to give accurate predictions for the experimental magnetic field, despite the fact that the calculated electric field bears little resemblance to the experimental electric field. In reality the e.m.f. is not uniformly distributed around the coil, but injected at a particular azimuthal location. In this light it is better to consider what is called the 'electric field', in this calculation, as proportional to the magnetic vector potential, rather than a physically observable quantity, and related by a gauge transformation to something approximating the experimentally measurable electric field.

4. Any ferrites are homogeneous, linear and isotropic. At a boundary where ferrite abuts metal the boundary condition of Eq. 5 is clearly valid. At a boundary that is between two non-metallic regions of different permeability, continuity of the H field tangential to the boundary implies

$$(\nabla_1 E_\phi.\hat{\mathbf{n}}_1 + \frac{E_\phi \hat{n}_{1r}}{r})\mu_2 = -(\nabla_2 E_\phi.\hat{\mathbf{n}}_2 + \frac{E_\phi \hat{n}_{2r}}{r})\mu_1 \ , \qquad (6)$$

where regions 1 and 2 have permeabilities μ_1 and μ_2. In the above $\hat{\mathbf{n}}_1$ is is the unit normal out of region 1. Clearly $\hat{\mathbf{n}}_1 = -\hat{\mathbf{n}}_2$. $\nabla_1 E_\phi$ is the gradient of the electric field on the region 1 side of the boundary. In addition to Eq. 5, there is of course the condition that E_ϕ is continuous across the boundary.

2.2 Integral Formulation

The simulation of the general antenna, under the above approximations, requires the solution of the partial differential equation, Eq. 3, subject to the boundary conditions, Eq. 5, on a set of closed metallic surfaces $\{m_i\}$ and, Eq. 6, on a set of ferrite surfaces $\{f_j\}$. The solution will be found by a boundary element method. One positive feature of this method is that the problem is set up to solve directly for the surface currents on metal parts, taking as input the e.m.f. on the coil. The surface currents are precisely what is required to compute the Ohmic losses. The boundary element method also greatly simplifies the specification and meshing of the antenna geometry. By means of Green's theorem, the following identity may be established:

$$E_\phi(\mathbf{x}) = \oint_{\{m_i\}} [E_\phi(\mathbf{x}_{m_i}) \nabla_{m_i} G(\mathbf{x}_{m_i}, \mathbf{x}).\hat{\mathbf{n}} - G(\mathbf{x}_{m_i}, \mathbf{x}) \nabla_{m_i} E_\phi(\mathbf{x}_{m_i}).\hat{\mathbf{n}}] \, \mathrm{d}\mathbf{x}_{m_i} - \int_{\{f_j\}} G(\mathbf{x}_{f_j}, \mathbf{x}) \lambda(\mathbf{x}_{f_j}) \, \mathrm{d}\mathbf{x}_{f_j} \ , \tag{7}$$

where $\hat{\mathbf{n}}$ is the unit normal into the surface m_i at position $\mathbf{x}_{m_i}$ and G is Green's function, satisfying

$$\nabla^2 G(\mathbf{x}, \mathbf{x}') - \frac{G(\mathbf{x}, \mathbf{x}')}{r^2} = \delta(\mathbf{x}' - \mathbf{x}) \ , \tag{8}$$

here r is the radial coordinate of the position vector $\mathbf{x}$. The function $\lambda(\mathbf{x}_{f_j})$ is defined by

$$\lambda(\mathbf{x}_{f_j}) \equiv \nabla_1 E_\phi(\mathbf{x}_{f_j}).\hat{\mathbf{n}}_1 + \nabla_2 E_\phi(\mathbf{x}_{f_j}).\hat{\mathbf{n}}_2 \ . \tag{9}$$

Eq. 7 may be simplified by inserting the known form of the electric field on the metallic surfaces given by Eq. 5, and performing an integration by parts. This yields

$$E_\phi(\mathbf{x}) = - \oint_{\{m_i\}} G(\mathbf{x}_{m_i}, \mathbf{x}) i(\mathbf{x}_{m_i}) \, \mathrm{d}\mathbf{x}_{m_i} - \int_{\{f_j\}} G(\mathbf{x}_{f_j}, \mathbf{x}) \lambda(\mathbf{x}_{f_j}) \, \mathrm{d}\mathbf{x}_{f_j} \ , \tag{10}$$

where the quantity $i(\mathbf{x}_{m_i})$ is defined by

$$i(\mathbf{x}_{m_i}) \equiv \tilde{\nabla}_{m_i} E_\phi(\mathbf{x}_{m_i}).\hat{\mathbf{n}}_{m_i} \ , \tag{11}$$

where the operator $\tilde{\nabla} \equiv \nabla + \hat{\mathbf{r}}/r$. Note that $i(\mathbf{x}_{m_i})$ is proportional to the surface current density on the metal.

A set of integral equations over the metal surfaces $\{m_i\}$ may be obtained by setting $\mathbf{x}$ in Eq. 10 to a point on the k-th metal surface, yielding

$$\frac{C_k}{r_{m_k}} = - \oint_{\{m_i\}} G(\mathbf{x}_{m_i}, \mathbf{x}_{m_k}) i(\mathbf{x}_{m_i}) \, \mathrm{d}\mathbf{x}_{m_i} - \int_{\{f_j\}} G(\mathbf{x}_{f_j}, \mathbf{x}_{m_k}) \lambda(\mathbf{x}_{f_j}) \, \mathrm{d}\mathbf{x}_{f_j} \ . \tag{12}$$

The set of coupled integral equations for the unknown functions i and λ may be completed by taking the gradient of Eq. 10 and using the boundary condition Eq. 6, yielding

$$\lambda(\mathbf{x}_{f_k})\frac{\mu_1+\mu_2}{2(\mu_1-\mu_2)} = -\oint_{\{m_i\}} \hat{\mathbf{n}}_1.\tilde{\nabla}_1 G(\mathbf{x}_{m_i},\mathbf{x}_{f_k}) i(\mathbf{x}_{m_i})\,\mathrm{d}\mathbf{x}_{m_i} - \int_{\{f_j\}} \hat{\mathbf{n}}_1.\tilde{\nabla}_1 G(\mathbf{x}_{f_j},\mathbf{x}_{f_k})\lambda(\mathbf{x}_{f_j})\,\mathrm{d}\mathbf{x}_{f_j}\ , \quad (13)$$

where $\hat{\mathbf{n}}_1$ is the unit surface normal at position $\mathbf{x}_{f_k}$ and the $\tilde{\nabla}$ operators are applied to the second argument of G.

2.3 Numerical Algorithm

The integral equations Eq. 13 and Eq. 12 uniquely determine the functions $\{\lambda_i\}$ and $\{i_i\}$. Once these have been found one can of course determine the electric and magnetic fields anywhere by use of Eq. 10 and its spatial derivatives. Up to the addition of terms that vanish when the azimuthal part of the surface integrals is performed, $G(\mathbf{x},\mathbf{x}') = -\cos(\phi-\phi')/4\pi|\mathbf{x}-\mathbf{x}'|$. $\{\lambda_i\}$ and $\{i_i\}$ are of course independent of ϕ, and thus by performing the azimuthal integral over G, Eq. 13 and Eq. 12 are reduced to a set of one dimensional coupled integral equations. By standard manipulations [3], the azimuthal integrals over G and its derivatives may be reduced to complete elliptic integrals. (Details are given in Appendix B.)

The algorithm chosen here represents the set of surfaces $\{f_j\}$ and $\{m_i\}$ by a set of functions of the form $\mathbf{x}_{s_k}(\epsilon_k)$ where ϵ_k is the arclength along the intersection line of the k-th surface with the $\phi=0$ plane, and $\mathbf{x}=(r,z)$ is the position vector of a point on that line in the $\phi=0$ plane. We may then re-write Eqs. 13 and 12 as

$$\begin{aligned}\frac{C_k}{r(\epsilon'_k)} &= -\int_0^{L_i} K_1(\epsilon'_k,\epsilon_i) i(\epsilon_i)\,\mathrm{d}\epsilon_i - \int_0^{L_j} K_1(\epsilon'_k,\epsilon_j)\lambda(\epsilon_j)\,\mathrm{d}\epsilon_j \\ \lambda(\epsilon'_k)\frac{\mu_1+\mu_2}{2(\mu_1-\mu_2)} &= -\int_0^{L_i} K_2(\epsilon'_k,\epsilon_i) i(\epsilon_i)\,\mathrm{d}\epsilon_i - \int_0^{L_j} K_2(\epsilon'_k,\epsilon_j)\lambda(\epsilon_j)\,\mathrm{d}\epsilon_j\end{aligned} \quad (14)$$

Note that the elliptic integrals contained in K_1 and K_2 are are logarithmically singular as $\epsilon'_i \to \epsilon_j$, if $i=j$ and if the function $\mathbf{x}_{s_i}(\epsilon)$

is smooth. The lines $\mathbf{x}_{s_k}(\epsilon_k)$ are divided into patches which can be of different size. On each patch four nodes are placed. If the arclength of the patch is $4h$ then the nodes are each a distance h apart, and the end nodes are $h/2$ from the ends of the patch. The functions λ_i and i_j are approximated by the cubic polynomials on each patch which run through the values of the functions at the 4 nodes. A linear system is then formed by point matching the primed coordinates in Eq. 14 at the nodes on the patches. The kernels are integrated numerically against the cubic polynomials using an adaptive Gauss-Kronrod routine. (The logarithmic singularity having been subtracted out and integrated against the polynomial analytically). It is emphasized that the geometrical curvature of the boundary surfaces is taken into account exactly in this algorithm, regardless of how many patches one chooses. The variation of the functions $\lambda(\epsilon)$, and $i(\epsilon)$ is of course not exact.

For the results in this paper, the patches along each separate piecewise smooth arc were usually taken equally spaced in terms of arclength. As a first guess this does well since it is very simple to take small patches around the circumference of thin wires, and larger ones elsewhere. For certain extreme geometries it was necessary to increase the density of patches near field concentrations to achieve high accuracy. To improve on this, it is a fairly simple matter to automate the code to adaptively refine the patch size in areas of current concentration. A nice implementation of such refinement of boundary elements is given in Helsing [4].

2.4 Conducting Media

As has already been mentioned, the above approach does not accurately model the antenna performance in the presence of conductive drilling fluids. In a conducting medium, Eq. 3 must be modified to

$$\nabla^2 E_\phi - \frac{E_\phi}{r^2} + k^2 E_\phi = 0 \,, \tag{15}$$

where $k^2 = i\omega\mu\sigma$, and σ is the conductivity of the medium.

Since part of the domain will be conductive, and part not, there is not one Green's function for the whole space and one cannot write down a single integral equation that determines E_ϕ everywhere. One strategy is to write down a separate integral equation for each region of separate σ and couple them together with the relevant boundary con-

ditions. This method requires evaluating integrals over each Green's function and its first and second spatial derivatives. These will be slow to evaluate in the conductive case, since the azimuthal integrals are no longer simple elliptic integrals.

A great simplification for the kind of geometry in question is that the conductive part of the geometry (the borehole and formation) is to a good approximation independent of z. In this situation, one may couple a so-called 1.5-dimensional solution in the exterior dissipative region, to the 2 dimensional interior solution. This is reasonable if the geometries of interest are limited to a cylindrical borehole of a given conductivity, surrounded by rock formation of a different conductivity. In the formation, i.e., for $r > r_f$, the solution to Eq. 15 may be written as

$$E_\phi(r,z) = \int e^{ik_z z} A(k_z) H_1^{(1)}(\kappa_f r)\,\mathrm{d}k_z \ , \tag{16}$$

where $H_1^{(1)}$ is a Hankel function, $\kappa_f = \sqrt{k_f^2 - k_z^2}$, and k_f^2 is the value of $i\omega\mu\sigma$ in the formation. In the borehole, i.e. for $r_f > r > r_b$, the solution is

$$E_\phi(r,z) = \int e^{ik_z z}[B(k_z) H_1^{(1)}(\kappa_b r) + C(k_z) H_1^{(2)}(\kappa_b r)]\,\mathrm{d}k_z \ . \tag{17}$$

Continuity of E_ϕ, and its radial derivative, at the edge of the formation, $r = r_f$, yields $C(k_z) = -\Gamma(k_z) B(k_z)$, where

$$\Gamma(k_z) = \frac{\kappa_f H_1^{(1)}(\kappa_b r_f) H_0^{(1)}(\kappa_f r_f) - \kappa_b H_0^{(1)}(\kappa_b r_f) H_1^{(1)}(\kappa_f r_f)}{\kappa_f H_1^{(2)}(\kappa_b r_f) H_0^{(1)}(\kappa_f r_f) - \kappa_b H_0^{(2)}(\kappa_b r_f) H_1^{(1)}(\kappa_f r_f)} \tag{18}$$

For $r < r_b$, E_ϕ satisfies Eq. 10, with the extra term,

$$\int_I [E(\mathbf{x}_I) \nabla . \hat{\mathbf{n}}_I G(\mathbf{x}_I, \mathbf{x}) - G(\mathbf{x}_I, \mathbf{x}) \nabla . \hat{\mathbf{n}}_I E(\mathbf{x}_I)]\,\mathrm{d}\mathbf{x}_I \ , \tag{19}$$

added to the right hand side. Here $\mathbf{x}_I$ are points in the $r = r_b$ surface on the interface between the non-conducting domain and the exterior conducting domain, thus $\hat{\mathbf{n}}_I = \hat{\mathbf{r}}$. The interface may not cover the entire $r = r_b$ surface, since in most cases r_b will be the outermost radius of the mandrel. The integral in (19) is only over the non-metallic portion of the $r = r_b$ surface, so that the metal

surfaces used in Eq. 10 combined with the interface in the extra term (19) together form a closed surface. The extra term (19) passes in an obvious way through to Eq. 12, and Eq. 13 which in some sense determine $i(\mathbf{x}_m)$ and $\lambda(\mathbf{x}_f)$, respectively. An integral equation which determines $\nabla.\hat{\mathbf{n}}_I E(\mathbf{x}_I)$ may be found by taking Eq. 10 combined with (19), and letting $\mathbf{x}$ approach the interface. This yields

$$\frac{E(\mathbf{x}'_I)}{2} = -\oint_{\{m_i\}} G(\mathbf{x}_{m_i},\mathbf{x}'_I) i(\mathbf{x}_{m_i})\,\mathrm{d}\mathbf{x}_{m_i} - \int_{\{f_j\}} G(\mathbf{x}_{f_j},\mathbf{x}'_I)\lambda(\mathbf{x}_{f_j})\,\mathrm{d}\mathbf{x}_{f_j} + \int_I [E(\mathbf{x}_I)\nabla.\hat{\mathbf{n}}_I G(\mathbf{x}_I,\mathbf{x}'_I) - G(\mathbf{x}_I,\mathbf{x}'_I)\nabla.\hat{\mathbf{n}}_I E(\mathbf{x}_I)]\,\mathrm{d}\mathbf{x}_I \ . \quad (20)$$

Finally, the field in the interface, $E(\mathbf{x}_I)$ may be eliminated from all equations by means of the exterior solution:

$$E(r_b,z_I) = \int e^{ik_z z_I}\partial_r\tilde{E}(r_b,k_z)\frac{H_1^{(1)}(\kappa_b r_b) - \Gamma(k_z)H_1^{(2)}(\kappa_b r_b)}{\kappa_b(\dot{H}_1^{(1)}(\kappa_b r_b) - \Gamma(k_z)\dot{H}_1^{(2)}(\kappa_b r_b))}\,\mathrm{d}k_z \ , \quad (21)$$

where $\dot{H}_1^{(n)}(x) = H_0^{(n)}(x) - H_1^{(n)}(x)/x$ and $\partial_r\tilde{E}(r_b,k_z) = \frac{1}{2\pi}\int e^{-ik_z z}.\partial_r E(r_b,z)$. This expresses the field in the interface in terms of $\partial_r E(r_b,z)$ for all z, not just z in the interface. Thus if part of the $r = r_b$ plane is along the mandrel, eliminating the field in the interface, $E(\mathbf{x}_I)$, has coupled in a new unknown function, $\partial_r E(r_b,z)$ on the mandrel. This function is determined by using the fact that $E(r_b,z) = 0$ on the mandrel. Allowing z to be on the mandrel in Eq. 21, and setting the left hand side to zero produces a further equation for $\partial_r E(r_b,z)$. It might seem more natural to use the exterior solution to eliminate $\partial_r E(r_b,z)$ on the interface in terms of E on the interface, which would not couple in a new unknown function. In fact the use of the exterior solution to eliminate variables from the interior is rather delicate numerically, and is discussed in appendix A. In any case, the apparently unnecessary direct computation of the surface currents on the exterior of the mandrel is actually convenient for computing the Ohmic losses there.

3. ANTENNA OPTIMIZATION

In this section the physics of certain design features of the type of antenna described in the introduction will be considered. The principles

will then be illustrated with results from the numerical code just described. Note that the geometrical lengths and other parameters used below have been chosen to illustrate physical principles and do not necessarily correspond to what is feasible for a practical antenna.

A useful measure of r.f. sensor performance, is the magnetic field that is produced in the rock formation divided by the square root of the power dissipated to produce that field. With this in mind, the antenna will be judged by its sensitivity defined as the magnitude of the z component of peak magnetic field produced at the location $r = 18''$, $z = 0$ divided by the square root of mean dissipated power, at 1MHz.

To make the discussion concrete, consider the simplified antenna geometry shown in Fig. 2. All metal surfaces in this model are taken to be of equal resistivity, $0.1802\Omega\,\mathrm{m}$. (Approximately right for copper.) The relative permeability of the ferrite is taken to be 100. The results of a numerical calculation for this geometry are shown in Fig. 3.

3.1 The Dimensions of the Antenna

A key constraint that must remain satisfied when considering variations in antenna parameters is that the antenna stay between certain fixed minimum and maximum radii. The minimum radius is based on the deepest recess that can be cut into the mandrel without causing structural failure. The maximum radius is derived from the fact that the antenna should not protrude into the borehole. Given that the radial dimensions are more or less fixed for mechanical reasons, the coarsest geometrical parameter available for change is the extent of the recess in the z-direction.

Consider stretching out the recess by increasing zo but keeping all other marked lengths fixed. It is clear that this can only decrease the magnetic reluctance of the antenna, and thus increase the inductance. A simple way to think about this is as follows. As zo increases, the surface area of ferrite through which flux lines can penetrate into the exterior region increases. The additional flux lines increase the inductance of the antenna. For high permeability ferrite, the flux lines exit the ferrite normal to its surface. In the crude approximation that the flux lines exterior to the ferrite are semi-circles, the extra flux from increasing zo will tend to penetrate to a distance of the order $r = rf + zo$ in the $z = 0$ plane. From these considerations, one would expect that as one stretches out the antenna the sensitivity will rapidly increase until $rf + zo \sim 18''$, after which there will only be small gains. This

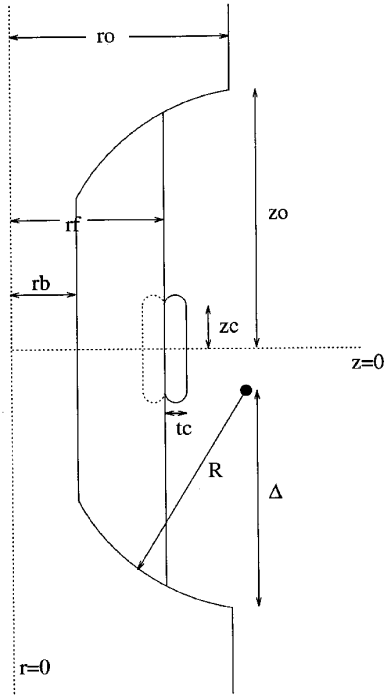

Figure 2. Simplified Antenna for Optimization. The current flows in the solid belt of copper that sits on top of a block of ferrite, which fills the remaining mandrel recess. The labeled geometrical parameters may each be varied independently but together completely determine the model. The dimensions chosen as a starting point for calculations are $zc = 0.5''$, $tc = 0.25''$, $rb = 9''$, $rf = 9.5''$, $ro = 10''$, $zo = 3''$, $R = 1''$, and $\Delta = 1''$. Note that all curved sections are taken to be circular arcs. The curved edges of the current belt are semi-circles. The dotted line marks the current belt embedded in the ferrite, as described in section 3.2.

behavior is illustrated in Fig. 4, which shows the effect of increasing zo on the numerically calculated sensitivity.

However, having stretched out zo, one can also stretch out the vertical extent of the current belt, by increasing zc. This can only decrease the magnetic field in the $z = 0$ plane. However the resistance of the copper belt decreases roughly as $1/zc$, so one can gain substantially in the sensitivity, $B/\sqrt{P}$, by increasing zc. One expects

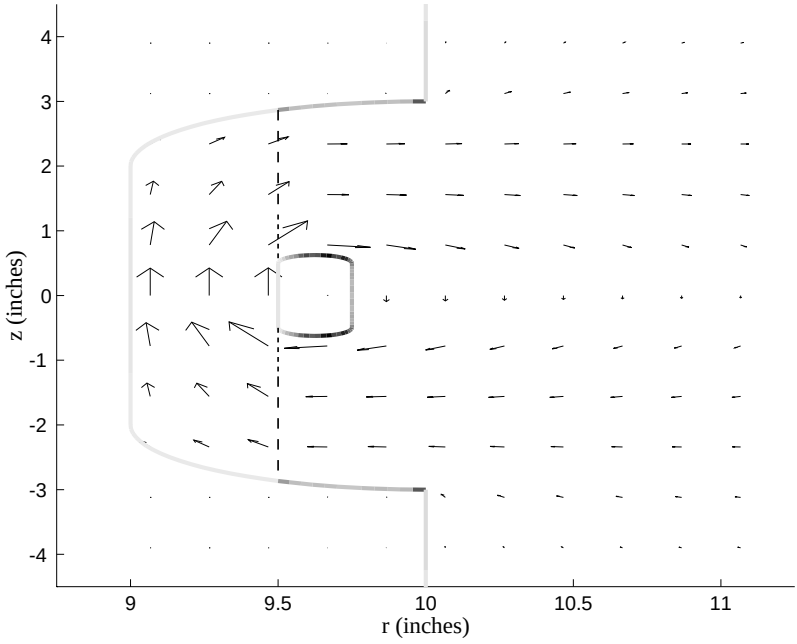

Figure 3. Solution for surface currents and field map of the simplified antenna shown in Fig. 2. The magnitude of the surface current density on metal parts is indicated by the darkness of the greyscale line. Note that the surface currents tend to bunch on the edges of the current carrying belt, and that there is very little surface current on metal parts which are next to ferrite. The boundary of the ferrite is indicated by the dotted line.

to gain until $zc \sim zo/2$, or $18'' - rf$, *whichever is smaller*. When zc is much larger than $zo/2$, it starts to substantially pinch off the magnetic field, and the inductance of the coil is decreased. (Of course when zc is so large that the coil touches the mandrel, the sensitivity must go to zero.) When zc is much larger than $18'' - rf$, the field lines penetrate unnecessarily deep beyond the $18''$ radius of interest, and efficiency is curtailed. Fig. 5 shows the combined effect of changing zo and zc together, calculated numerically. The plot shows that in principle antennas with efficiencies of over $0.2\text{Gauss}/\sqrt{\text{Watt}}$ are possible. In practice it would be difficult to engineer a sufficiently robust shield

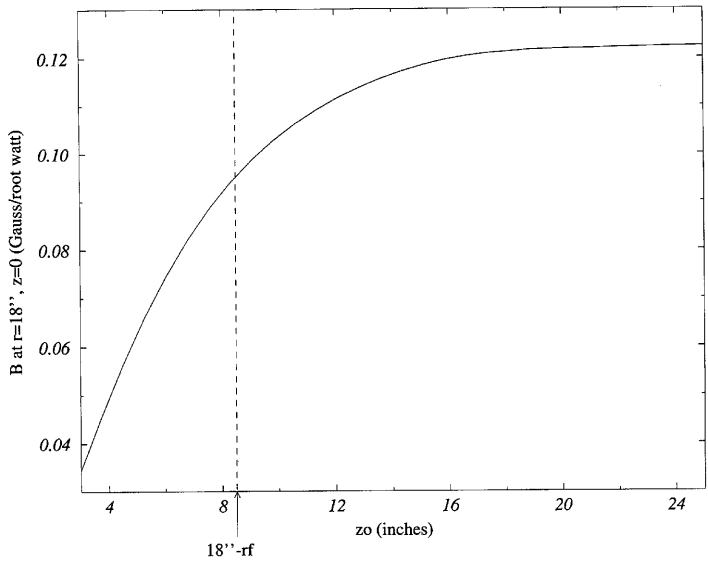

Figure 4. The effect of increasing zo on the simplified antenna of Fig. 2. The sensitivity starts to level out after $rf + zo \sim 18''$.

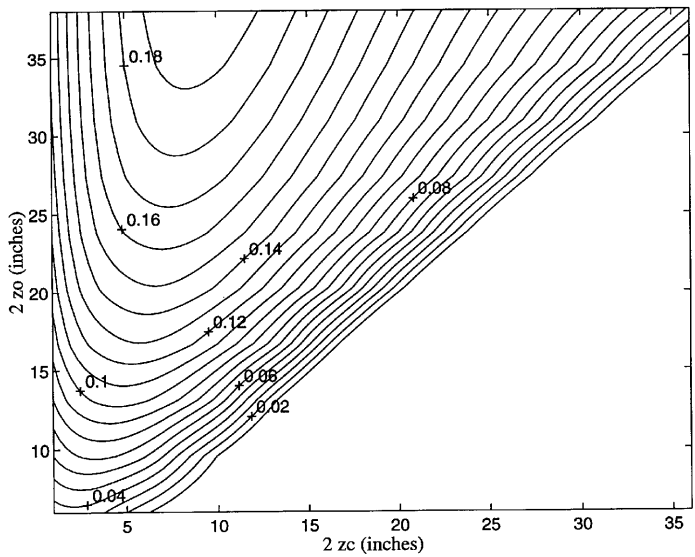

Figure 5. The effect of varying zc and zo on the simplified antenna of Fig. 2. The contours are of B at $r = 18''$, $z = 0$, in Gauss $/\sqrt{\text{Watt}}$.

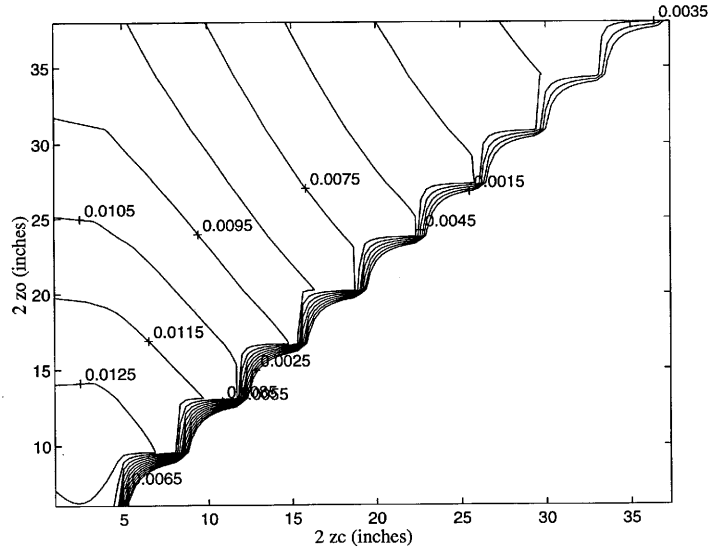

Figure 6. The effect of varying zo and zc with a $1\Omega^{-1}m^{-1}$ conductivity borehole. The contours are of B at $r = 18''$, $z = 0$, in Gauss $/\sqrt{\text{Watt}}$. The conductivity of the rock formation is taken to be one tenth the borehole value. The radius of the formation is taken to be $14''$. Note that the oscillation at $zo \sim zc$ is an artifact produced by the contour plotting routine.

to protect such stretched antennas from the borehole environment. In addition, the effect of borehole salinity has not been considered, so far. Fig. 6 shows that Fig. 5 can be radically changed in the presence of a conductive borehole. Despite the conductive borehole, increasing zo can still only increase the magnetic field produced by the antenna. However, such stretched antennas produce a far greater volume of electromagnetic field. This means much more power is dissipated in the borehole and the overall sensitivity, $B/\sqrt{P}$, now falls off for large zo, as can be seen in Fig. 6. At this borehole conductivity there is clearly an optimal antenna size.

3.2 The Effect of Ferrite.

Once the overall dimensions of the antenna are fixed, there are of course many small scale design parameters that can be adjusted to improve performance. It will now be shown that several of these small

scale features are driven by the fact that the permeability, μ, of the ferrite is very large. In particular, the value of μ that is commercially available results in in a remarkable flexibility of certain geometrical parameters.

The main purpose of filling the mandrel recess with ferrite, as stated in the introduction, was to lower its magnetic reluctance. (In other words to increase the flux through the coil for a given current). In practice the ferrite has other effects. Linked to the lowering of the magnetic reluctance is the effect that the ferrite tends to expel current. More precisely the surface currents on a metal edge that is flush with ferrite, tend to be much smaller than on a metal edge that is outside the ferrite. One way to understand this is that the current per unit length on a metal boundary in the r - z plane is proportional to B/μ. If we cross into ferrite, as we travel along a metal boundary, and B does not change by a large amount, (compared to $\mu \sim 100$), then the surface current will drop by a large factor. This fact has several consequences when considering even the simple antenna of Fig. 2.

First consider the coil, which is represented by a copper belt in Fig. 2. It is well known that a.c. current on a thin belt tends to concentrate at the edges of the belt, causing high power loss. If the belt were to be bedded into the ferrite, as is shown by the dotted line in Fig. 2, the ferrite would push the current away from the edges onto the outer face of the belt, decreasing the power loss. Furthermore, if the coil is bedded in the ferrite, nearly all the current is flowing on the outer face of the coil, therefore the antenna sensitivity is only very weakly dependent on the coil thickness, tc. Table 1 shows the effect of bedding the coil and drastically decreasing tc, by a factor of 10.

	Belt Outside Ferrite, $tc = 0.25''$	Belt Bedded in Ferrite, $tc = 0.25''$	Belt Bedded in Ferrite, $tc = 0.025''$
$zo = 3''$ $zc = 1''$	0.0367	0.0382	0.0376
$zo = 6.56''$ $zc = 2.18''$	0.103	0.116	0.115
$zo = 10.1''$ $5\,zc = 3.37''$	0.149	0.174	0.175

Table 1. The Effect on Antenna Sensitivity (in Gauss $/\sqrt{\text{Watt}}$) of Bedding the Current Belt in the Ferrite. Unless specified otherwise, the geometry and all length scales are those in Fig. 2.

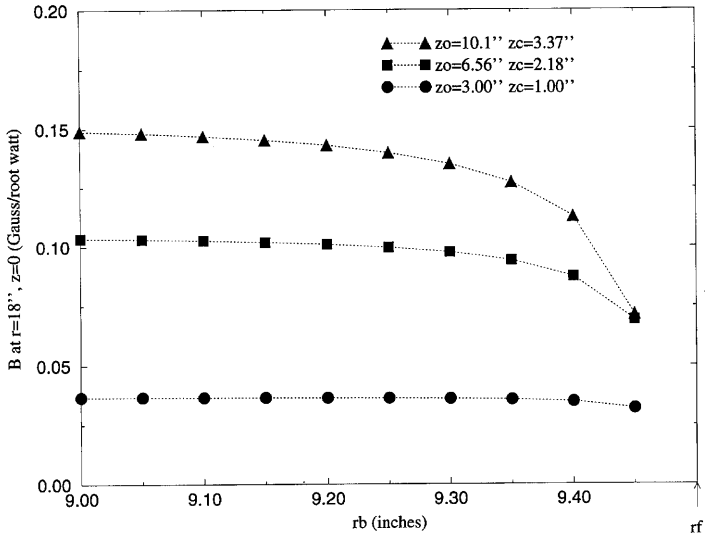

Figure 7. The effect of decreasing ferrite thickness on three different antennas. All unmarked dimensions are as in Fig. 2. $\mu = 100$.

Now consider the depth of the mandrel recess. Since very little current flows on the mandrel behind the ferrite, the recess can be made very shallow, with little effect on the antenna performance. (Alternatively the ferrite can be made very thin.) The effect of increasing rb, leaving other dimensions constant is shown in Fig. 7.

For finite μ, if the ferrite layer is thin enough, antenna sensitivity will start to suffer. This is because if one distorts the geometry enough, the magnetic field inside the ferrite becomes very different to that outside. Consider surface currents on the mandrel. The magnetic field next to the mandrel, inside the ferrite, will be largest at $z = 0$, since this is the narrowest constriction the field must pass through. The magnetic field next to the mandrel, outside the ferrite, will be largest right where the field lines exit the ferrite, since the field lines tend to spread out after this point. Let us denote the z-coordinate of the point where the ferrite meets the mandrel as zf. A crude approximation to the ratio of maximum magnetic fields interior to the ferrite to those exterior to the ferrite is given by $(zf - zc)/(rf - rb)$. (If the current belt is now back outside the ferrite.) Only when this number approaches μ, will the surface currents on the mandrel behind

the ferrite become roughly the same size as those on the mandrel exterior to the ferrite. This explains how remarkably thin the ferrite can become before antenna performance is affected. For the lowest curve in Fig. 7, this ratio ranges from 4 to 37, at the most extreme right hand point. This is still significantly smaller than $\mu = 100$, and so the antenna sensitivity has not changed much. For the next two curves up, for which $zf - zc$ is larger, $(zf - zc)/(rf - rb)$ ranges from 8 to 85 and 13 to 132 respectively. This ratio is now comparable to or greater than μ, on the right hand side of the graph, and so the sensitivity of the upper two antennas has been significantly affected by the narrowing of the ferrite layer.

A simple rule of thumb for how thin one can make the current belt without incurring loss is less obvious. This is because there tend to be complicated concentrations in magnetic field around the edges of the belt.

3.3 Coil Composition

So far the antenna coil has been simplified to a single turn copper belt. It is natural to ask if a coil can do better. This issue turns out to be a rather complicated problem, dominated by 'proximity' effects, but can have significant impact on the sensitivity of the antenna. The physics is very similar to that of a long multiwire transmission line, first treated in detail by Smith [1].

The details of the coil are unlikely to affect the magnetic field relatively far away in the rock formation, thus the emphasis here is on how the coil should be built to minimize the dissipated power. The problem with the single turn belt that has been considered so far is that the a.c. current tends to concentrate at the edges of the belt, causing high power dissipation. If the current could be distributed more uniformly over the surface of the belt then the dissipated power for a given current would decrease. In the cylindrical symmetry approximation, a coil is thought of as a series of metal hoops, with the current constrained to be equal on each hoop. Since as much current is forced to flow in the center hoops of the coil as flows in the outer hoops, use of a coil appears to solve the problem of distributing the current more evenly. In fact this is not the case due to the mutual inductive repulsion of the surface currents on neighboring wires in the coil.

Insight may be gained by considering a long straight wire of circular cross-section, radius R, much greater than the skin depth, carrying a

total a.c. current, I, at high frequency. The current of course flows in a thin skin on the surface of the wire, and due to symmetry is evenly distributed around the circumference of the wire. The surface current per unit length of circumference is $i = I/(2\pi R)$. The dissipated power per unit length is proportional to $\int i^2 = (2\pi R) \times (I/2\pi R)^2 = I^2/2\pi R$. A naive observation would be that since the dissipated power is high, because all the current is confined to the surface, one would gain by placing a thin insulating cylindrical sheath in the wire at radius $R/2$ and forcing some fraction, x, of the total current down the center core of the wire, and $(1-x)I$ down the outer annulus. One can see immediately that this only makes things worse. The power dissipated on the inner cylinder is $\sim x^2 I^2/\pi R$. The problem arises in the annulus where in order to have both zero magnetic field in the middle of the annulus, and satisfy Ampere's law, there must be a negative current on the inside perimeter of the annulus, equal to xI. Thus on the inner surface of the annulus the dissipated power is also $\sim x^2 I^2/\pi R$. Because of the negative current on the inner surface, the total current on the outer surface of the annulus is still I and the dissipated power here is still $\sim I^2/2\pi R$. Thus by constraining a fraction x of the current to flow down the center of the wire, the dissipation has gone up by $\sim 2x^2 I^2/\pi R$.

A similar effect occurs when one splits up the copper belt shaped wire of roughly rectangular cross section into say eight toroidal wires, and forces $I/8$ down each one. (This approximates using an eight turn coil.) More precisely consider the geometry shown in Fig. 2, with $zo = 3''$, and $zc = 1''$, but with the current belt replaced by eight equally spaced copper hoops, of diameter $tc = 0.25$ inches, each hoop carrying the same current. The cross section of the coil in the r-z plane is now more similar to that in Fig. 1. (Although the coil is not bedded in the ferrite.) To simplify the numerics, the coil was slightly spaced off the surface of the ferrite by $0.005''$. The center of the uppermost hoop is at $r = rf + tc/2 + 0.005''$, $z = 1''$.

The center of the next hoop down is at $r = rf + tc/2 + 0.005''$, $z = 2.5/3.5''$, and so on for the other hoops. All other dimensions are as given in Fig. 2. The distribution of surface currents on the upper four wires of such a coil is shown in Fig. 8. Although the outermost wires do not screen the inner ones to the extent given in the simple example above, the current distribution over their surface becomes extremely non-uniform. One way to understand Fig. 8 is to note that the surface

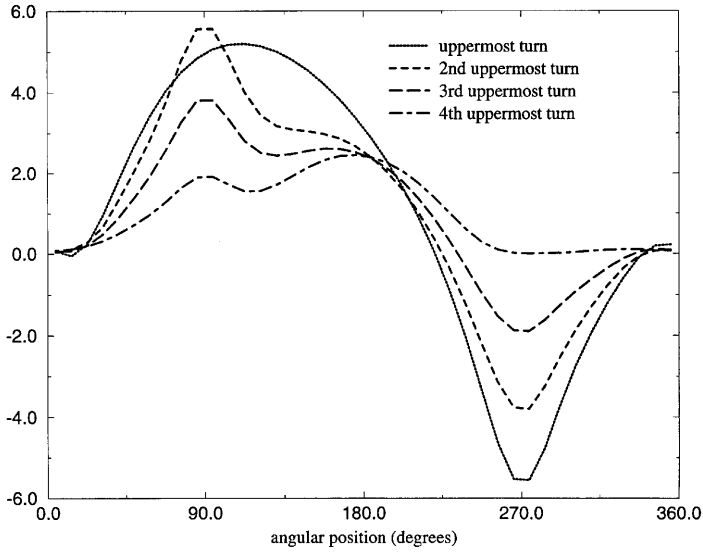

Figure 8. The current densities on the surface of the upper four loops of the eight turn coil antenna described in the text. The cross section of a loop in the r-z plane forms a circle, and the angular position referred to in the figure is measured clockwise around this circle. The point of zero angle is defined to be the point of smallest radial position – i.e., the point closest to the ferrite surface.

currents on the wires repel each other inductively in a similar manner to electric charges repelling each other electrostatically. The center turns of the coil are surrounded roughly symmetrically by the other turns of the coil and thus have a more uniformly distributed surface current. By contrast the upper most turn has only current flowing beneath it, and so the current it carries is pushed onto its uppermost face, and sufficiently strongly that negative currents are left on its lower face. This kind of behavior was seen in the work by Smith [1]. The situation dealt with here is further complicated by the presence of ferrite which tends to push both positive and negative currents away from the ferrite surface.

The result of the proximity effects between the wires leads to increased losses for an 8 turn coil as compared to a solid copper belt. The sensitivity of this antenna, except with the solid copper belt, was 0.0366 Gauss $/\sqrt{\text{Watt}}$ (c.f. Table 1). In the eight turn version, this

decreases to 0.0288 Gauss $/\sqrt{\text{Watt}}$, a loss of 26%. It is reasonable to expect that a four turn coil occupying the same space might be better, since the extra space between the turns should reduce the proximity effects and negative currents. A four turn antenna may be constructed by taking four equally spaced hoops of diameter $tc = 0.25$ inches. The center of the upper most hoop is still at $r = rf + tc/2 + 0.005''$, $z = zc$. The next one down is now at $r = rf + tc/2 + 0.005''$, $z = zc \times 1.5/2.5$, and so on. The numerical solution of this antenna still shows some negative currents on the outer two hoops, but the situation is not nearly as bad as the eight turn antenna. The sensitivity is 0.0353 Gauss $/\sqrt{\text{Watt}}$, only 4% worse than the solid copper belt.

These results suggest that proximity effects between wires are very significant when considering the antenna coil design. It appears that a single turn coil may well be the optimal configuration, although we have no proof of this. With care, it appears that multiturn antennas can be constructed with performance close to that of the single turn case. In addition, it should be noted that there are practical concerns in a real working device which have not been addressed here. In particular the inductance of the coil is strongly affected by the number of coil turns. This makes coupling into a single turn antenna problematic.

4. CONCLUSION

A boundary integral method has been developed which is capable of modelling certain near field radio frequency antennas. The antennas must be cylindrically symmetric, but otherwise can be quite complex. The method has been extended to model the effect of coupling the antennas to a lossy medium such as a borehole drilled for geophysical investigation.

The numerical method was used to explore quantitatively the physics of such an antenna. First the problem of how to choose the correct axial dimensions of such an antenna was considered. Then it was shown that the large permeability of ferrite materials available for use in such antennas results in remarkable design flexibility. Finally the coil composition was discussed. 'Proximity' effects between the turns of the coil were shown to have a substantial effect on antenna performance. It is suggested that under ideal conditions, a single turn coil has the smallest Ohmic losses for a given magnetic field.

ACKNOWLEDGEMENTS

The author would like to thank Apo Sezginer for his encouragement, and for suggesting the topic, and Pabitra Sen for useful discussion. Bert Halperin pointed out the analogy between proximity effects and currents in concentric long wires.

APPENDIX A.

In appendix A, strategies for eliminating variables from the interior dissipation free region using the exterior 1.5-dimensional solution are discussed. This process has difficulties, if one wants to keep the flexibility of spatially local basis functions. For simplicity, let the rock formation have identical properties to the borehole. The exterior solution is then

$$E(r,z) = \int e^{ik_z z} B(k_z) H_1^{(1)}(\kappa_b r)\,\mathrm{d}k_z \quad r > r_b \tag{22}$$

To make the example concrete, consider the antenna in Fig. 2. If the conducting fluid is flush with the mandrel, then $r_b = ro$ and the interface to the interior region is along $r = r_b\,,\ |z| < zo\,,$ elsewhere along $r = r_b$ there is metal with $E = 0\,.$ The problem is how to eliminate variables from the interior solution along the interface, using the exterior solution. The most natural way to parameterize the interior solution is in terms of E and $\tilde{\nabla} E.\hat{\mathbf{n}}\,.$ (Note that $\tilde{\nabla} E.\hat{\mathbf{n}} = \partial_r E + E/r \propto B_z\,.$) Thus for $|z| < zo$ we have $E(r_b,z) = \sum a_n f_n(z)\,,$ and $\tilde{\nabla} E.\hat{\mathbf{n}}(r_b,z) = \sum b_n f_n(z)\,.$ The interface $r = r_b\,,\ |z| < zo$ is divided into patches, and each basis function $f_n(z)$ is a polynomial in z on one of the patches, and zero elsewhere.

First consider eliminating $\tilde{\nabla} E.\hat{\mathbf{n}}$ from the interior solution, by writing

$$\sum_n b_n f_n(z) = \sum_m a_m \int e^{ik_z z} \tilde{f}_m(k_z) \frac{\kappa_b H_0^{(1)}(\kappa_b r_b)}{H_1^{(1)}(\kappa_b r_b)}\,\mathrm{d}k_z\,. \tag{23}$$

This has the advantage of eliminating the variables $\{b_n\}$ just in terms of $\{a_n\}\,,$ and not coupling any new unknowns into the interior solution. The drawback with this technique is that the function that is being Fourier transformed in Eq. 23 goes like $k_z \tilde{f}(k_z)$ for large $k_z\,.$ Since $f(z)$ is a local polynomial and thus a discontinuous function of $z\,,$

$\tilde{f}(k_z)$ falls off only as $1/k_z$, and the Fourier transform above does not converge. This problem is not easily solved by taking a local basis set that is continuous. In this case the integral still diverges for any z where the derivative of the basis function is discontinuous. This makes the use of triangle basis functions, which are continuous, but not smooth, problematic. The simplest solution to this difficulty is to eliminate E in the interface in terms of $\tilde{\nabla} E.\hat{\mathbf{n}}$,

$$\sum a_n f_n(z) = \sum b_m \int e^{ik_z z} \tilde{f}_n(k_z) \frac{H_1^{(1)}(\kappa_b r_b)}{\kappa_b H_0^{(1)}(\kappa_b r_b)} \, \mathrm{d}k_z \; . \qquad (24)$$

Note that now one has to expand the basis set $\{f_n\}$ to include $|z| > zo$. For the new basis functions the coefficients a_n are zero, but the b_n are non-zero, and are new unknowns that have been coupled into the problem. However the integrals clearly now converge at large k_z. Unfortunately a new difficulty emerges at small k_z. If a basis function has a spatial extent h, then it is likely, or certainly possible, that $h\kappa_b(k_z = 0) = hk_b$ is a small quantity. In this situation, the Fourier integral in Eq. 24 is very large, (infinite if $k_b = 0$), and is dominated by a large peak around $k_z = 0$. This reflects the fact that $\tilde{\nabla}\tilde{E}(r_b, k_z = 0) \propto \oint \mathbf{B}.\mathrm{d}\mathbf{l}$, where the contour of integration is up the z-axis at $r = r_b$ and closed at infinity. From Ampere's law this is the total azimuthal current flowing in the exterior region, which is very small if k_b is very small. The large peaks near $k = 0$ in the integrals in Eq. 24 are caused by the fact that local basis functions do not individually satisfy the global constraint that $\oint \mathbf{B}.\mathrm{d}\mathbf{l} \sim 0$. The numerical effect is that this one feature swamps everything else. The final solution has $\oint \mathbf{B}.\mathrm{d}\mathbf{l} \sim 0$ along the interface as required, but all detail is lost, because the central peak completely dominated the all the Fourier integrals in Eq. 24. This problem is circumvented by the slightly unnatural, but numerically stable, re-parameterization described in the main text. Here the interior solution is parameterized in terms of E and the $\nabla E.\hat{\mathbf{n}}$ and E is eliminated in terms of $\nabla E.\hat{\mathbf{n}}$.

APPENDIX B. ELLIPTIC INTEGRALS

This appendix details the reduction of the azimuthal integrals to elliptic functions. As mentioned in the main text, up to terms which vanish on performing the azimuthal integrals, the Greens function is given by $G(\mathbf{x}, \mathbf{x}') = -\cos(\phi - \phi')/4\pi|\mathbf{x} - \mathbf{x}'|$. In order to calculate the

kernel K_1 in Eq. 14 one must evaluate

$$K_1(\epsilon', \epsilon) = \int_0^{2\pi} Gr \, \mathrm{d}\phi = -\frac{\sqrt{r}}{2\pi\sqrt{2r'}} \int_0^{\pi} \frac{\cos\phi \, \mathrm{d}\phi}{\sqrt{a - \cos\phi}} \,, \tag{25}$$

where $a \equiv (r^2 + r'^2 + (z - z')^2)/(2rr')$. In addition it is necessary to compute derivatives of this integral with respect to the spatial variables $r\,, r'\,, z\,,$ and z'. The kernel K_2 in Eq. 14 involves first derivatives. Eq. 19, when carried through to Eq. 13 involves azimuthal integrals over second derivatives of G. The integrals that result from taking these derivatives are all of the form

$$I_n^m = \int_0^{\pi} \frac{\cos^m \phi \, \mathrm{d}\phi}{(a - \cos\phi)^{\frac{2n-1}{2}}} \,, \tag{26}$$

where n runs from 0 to 3 and m runs from 0 to n. Since $I_n^{m+1} = aI_n^m - I_{n-1}^m$ we only need be concerned with I_n^0, where n runs from 0 to 3. Using standard methods [3] the following identities may be established:

$$I_0^0 = 2\sqrt{1+a}\,\mathrm{E}(\bar{a}) \tag{27}$$

$$I_1^0 = \frac{2}{\sqrt{1+a}}\,\mathrm{K}(\bar{a}) \tag{28}$$

$$I_2^0 = \frac{2\,\mathrm{E}(\bar{a})}{\sqrt{1+a}(a-1)} \tag{29}$$

$$I_3^0 = \frac{2}{3}\frac{1}{\sqrt{1+a}(a^2-1)}\left[\frac{4a}{a-1}\mathrm{E}(\bar{a}) - \mathrm{K}(\bar{a})\right] \,, \tag{30}$$

where $\bar{a} \equiv 2/(1+a)$, and E and K are the usual complete elliptic integrals.

REFERENCES

1. Smith, G. S., *J. Appl. Phys.,* Vol. 43, 2196, 1972.
2. See for example Landau and Lifshitz, *Electrodynamics of Continuous Media*, Chapter VII, Pergamon Press, Oxford, 1960.
3. See for example M. Abramowitz and I. A. Stegun, *Handbook of Mathematical Functions*, Dover, New York, 1965.
4. Helsing, J., *J. Comp. Phys.,* Vol. 127, 142, 1996.